Frequency dependent signal transfer in neuron transistors

Rolf Weis and Peter Fromherz*
Department of Biophysics, University Ulm, D-89086 Ulm, Germany
and Department of Membrane and Neurophysics, Max-Planck-Institute for Biochemistry, D-82152 Martinsried, München, Germany
(Received 24 July 1996)

Nerve cells are attached to open, metal-free gates of field-effect transistors submersed in electrolyte. The intracellular voltage is modulated by small ac signals from 0.1 Hz to 5000 Hz using a patch-clamp technique. The source-drain current is affected in amplitude and phase through a modulation of the extracellular voltage in the cleft between transistor and cell. The ac-signal transfer is evaluated on the basis of linear response theory. We use the model of a planar two-dimensional cable which consists of the core of an electrolyte sandwiched between the coats of a cell membrane and silicon dioxide of the transistor surface. Comparing experiment and model we obtain the resistances of core and coat, i.e., of the seal of cell and surface and of the attached membrane. The resistance of the membrane varies in different junctions. It may be lowered by two orders of magnitude as compared with the free membrane. This drop of the membrane resistance correlates with an enhancement of the seal resistance, i.e., with closer adhesion. The linear ac-transfer functions are used to compute the signal transfer of an action potential. The computed response is in good agreement with the observations of excited nerve cells on transistors. [S1063-651X(97)13801-6]

PACS number(s): 87.22.−q, 73.40.Mr, 87.80.+s

I. INTRODUCTION

In a neuron transistor the elementary units of brains are connected directly to the elementary elements of computers [1]. Voltage transients across a cell membrane modulate the source-drain current through the insulating silicon dioxide of an open gate without the flow of electrochemical current across the interface [2]. It was possible, also, to reverse the coupling and to stimulate a neuron through the insulating silicon dioxide in an appropriate microstructure [3]. Such neuron-silicon junctions may be the basis for the development of hybrid networks for technological and medical application. However, as a next step we have to achieve a better understanding of the physics of the signal transfer in order to optimize the junctions for large-scale integration.

The setup of a neuron transistor is shown in Fig. 1. An individual neuron is attached directly to a metal-free insulated-gate field-effect transistor. Silicon and neuron are surrounded by an electrolyte kept on ground potential. A change of the intracellular voltage V_M affects the voltage in the junction area and modulates the source-drain current of the transistor at its working point. Two kinds of signals were observed as a response to an action potential in the neuron [2], a weak biphasic signal which resembles the damped first derivative of the intracellular voltage (an *A*-type junction) and a strong monophasic signal which resembles the action potential in its shape with an amplitude up to 30% (a *B*-type junction). Usually a given assembly has the features of an *A*-type or a *B*-type coupling. Intermediate couplings (*AB* type) are rare.

In a previous paper [4] we presented experimental data on the transfer of ac signals which suggested that an intact cell membrane is attached to the gate in an *A* junction whereas in the *B* junction the conductance of the membrane might be enhanced by the attachment. The interpretation was ambiguous because the data were reliable only up to about 1000 Hz.

In this paper we describe an improved experimental technique: We use a single electrode patch clamp which avoids damage of the neuron. We measure, in this configuration, the voltage modulation V_P in the patch pipette, the current I_P through the pipette, and the modulation of the source-drain

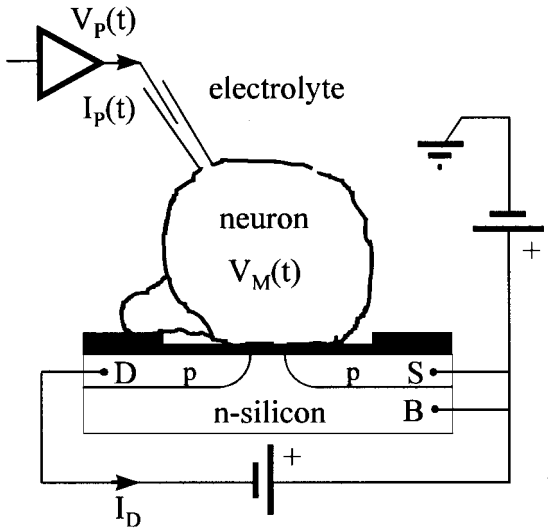

FIG. 1. Neuron transistor. A nerve cell in electrolyte is attached to a metal-free insulated-gate field-effect transistor. The channel is of *p* type. Bulk silicon (*B*), source (*S*), and drain (*D*) are kept on a positive voltage with respect to the electrolyte. The cell is fused to a patch pipette. A voltage V_P, with respect to ground, is applied to the pipette. As a result a current I_P flows into the pipette which affects the voltage V_M across the cell membrane. This intracellular voltage modulates the voltage in the junction between the membrane and the silicon dioxide which controls the source-drain current I_D in the transistor.

*Author to whom correspondence should be addressed. Electronic address: fromherz@biochem.mpg.de

current I_D. Using three two-phase lock-in amplifiers we attain a better signal-to-noise ratio. On the basis of these data we are able to determine the complex voltage transfer from the neuron to the gate in a range from 0.1 Hz up to 5000 Hz and to evaluate simultaneously the impedance spectrum of the neuron. We present a thorough theoretical description of the neuron-silicon junction which relies on the physics of a two-dimensional cablelike structure as used in a recent paper [5]. The evaluation of amplitude and phase of voltage transfer allows us to elucidate the nature of coupling in a neuron transistor.

We are aware that the model of a two-dimensional cable remains somewhat formal as long as no independent structural data on the neuron-silicon junction are available. The situation will change when the method of fluorescence interference contrast microscopy in Ref. [6] will allow a mapping of the distance between membrane and gate.

Unspecified interaction of neural excitation and transistors was reported some time ago. In 1976 Bergveld, Wiersma, and Meertens placed a transistor with an open gate into a tissue and observed a modulation of the source-drain current [7]. They did not define the potential of the silicon device with respect to the tissue. The size of the gate was by two orders of magnitude larger than a nerve cell. In 1981 Jobling, Smith, and Wheal inserted transistors with a metallized gate into a neural tissue [8]. It is the crucial issue of the previous studies on neuron transistors [2–5] and of the present paper that a close contact is made between an individual nerve cell and an individual transistor under well defined control of the electrical conditions of both elements.

In the first part of this paper we present the theoretical framework of the neuron transistor using concepts of the cable theory. Then we describe the experimental setup and the approach to measure impedance and voltage transfer. On this basis we consider three different neuron transistors which represent an *A*-type and a *B*-type junction and an intermediate *AB*-type coupling. Finally the ac-transfer functions are used to compute the signal transfer of the action potential of an excited neuron.

II. THEORY

In this section we describe the theory of neuron-silicon junctions as a basis for design and interpretation of the experiments. First we note crucial features of transistors and membranes in a linear approximation. Then we introduce the concept of a two-dimensional ''sandwich cable.'' We derive the pertinent cable equation and solve it for a simple geometry. Finally we consider the reduced model of a ''point contact.''

We decompose the neuron-silicon coupling in a neuron transistor in two parts: (i) A voltage profile is formed in the junction between cell membrane and silicon chip which depends on the neural stimulation and on the geometry and the electrical properties of the junction. (ii) This voltage affects the source-drain current in an open transistor as described by the current-voltage relationship at its working point.

Wet transistor. In a common metal-oxide-semiconductor (MOS) field-effect transistor (FET) the source-drain current is controlled by the voltage applied to the gate, which is a metal electrode. The change of the source-drain current in the silicon is proportional to the change of the gate voltage for small signals around the working point with appropriate bias voltages. The metallic gate can be replaced by a conductive electrolyte. In a neuron transistor we keep the bulk silicon, the source and the drain on defined voltages with respect to the bath on ground potential (Fig. 1). Any change of the local voltage on the gate—as caused in a neuron-silicon junction by neuronal activity—modulates the source-drain current as in a usual MOS-FET configuration. Thus an open transistor probes the local time-dependent voltage $V_J(x,y,t)$ in the junction. If the open gate is large we have to evaluate a certain average of the voltage profile.

Neuron membrane. The total current through a plasma membrane is a superposition of the capacitive current and of ionic currents through specific ion channels. With the specific capacitance c_M of the membrane and with the specific conductance g_M^i for the ion species i we obtain the current density

$$j_M = c_M \frac{dV_M}{dt} + \sum g_M^i (V_M - V_0^i). \tag{1}$$

At a given intracellular voltage V_M the ionic current is driven by the difference of that voltage and of the reversal voltage V_0^i which originates in unequal concentrations of ions across the membrane and in selective conductances of the ions channels.

In general the conductances g_M^i depend on the voltage V_M. They exhibit an autonomous dynamics as described, e.g., by the classical Hodgkin-Huxley equations [9]. In the present investigation we keep the membrane at a holding voltage which is around the intrinsic resting voltage of the neurons and superpose ac voltages of small amplitude. Thus we take care that the membrane voltage is beyond the range where the nonohmic features become important. Rewriting the current in terms of the total conductance g_M and of the resting voltage V_R we obtain Eq. (2). We assume $g_M = \text{const}$ around the holding voltage

$$j_M = c_M \frac{dV_M}{dt} + g_M (V_M - V_R),$$

$$g_M = \sum g_M^i, \quad V_R = \frac{\Sigma g_M^i V_0^i}{g_M}. \tag{2}$$

If the neuron is stimulated with an ac voltage of an amplitude $\underline{V}_M(\omega)$ at an angular frequency ω, the battery V_R plays no role and we obtain for the complex current

$$\underline{j}(\omega) = (g_M + i\omega c_M)\underline{V}(\omega). \tag{3}$$

Sandwich cable. When a neuron is attached to the surface of oxidized silicon, a conductive cleft of electrolyte is left between neuron and chip. It is insulated from the conductive silicon by silicon dioxide and from the conductive cell plasma by the plasma membrane, as illustrated in Fig. 2(a). This junction has the features of a cable: The cleft forms a core and the silicon dioxide and the membrane form the coats. We call this arrangement a ''sandwich cable.''

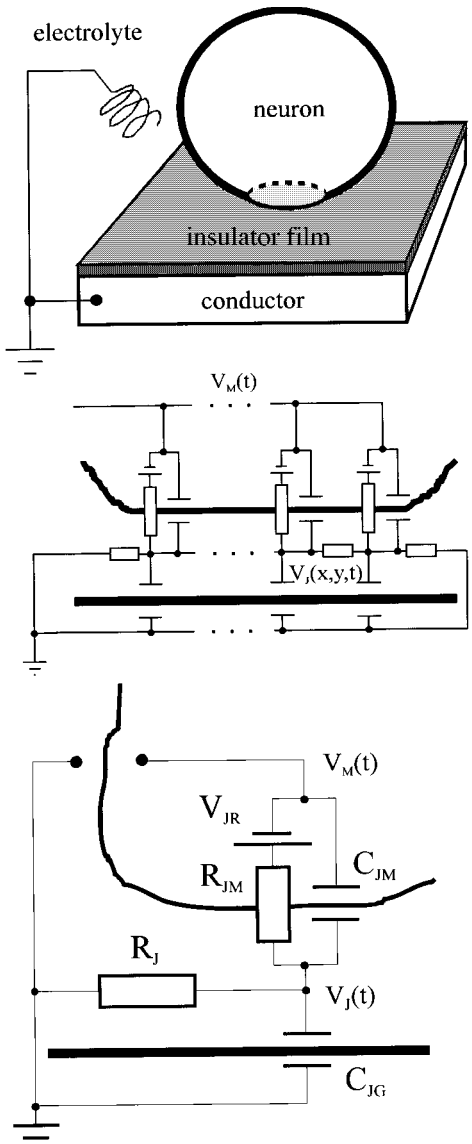

FIG. 2. Sandwich cable. (a) Structure. A cell membrane between the conductive cell plasma and the bulk electrolyte is attached to an insulating film (silicon dioxide) on a conducting substrate (silicon). (b) Circuit with differential elements: Specific capacitance of the membrane c_{JM}, specific conductance of the membrane g_{JM}, battery V_{JR}, specific capacitance of silicon dioxide c_{JG}, and sheet resistance r_J. The system is driven by the time-dependent voltage $V_M(t)$ in the cell. The response is a time-dependent voltage profile $V_J(x,y,t)$ in the two-dimensional core. (c) Point-contact model with capacitance and resistance C_{JM} and R_{JM} of the membrane, with the battery V_R, with the capacitance of silicon dioxide C_{JG} in the junction and with the seal resistance R_J. The bias voltage of the silicon is indicated.

We may visualize the sandwich cable by the circuit of Fig. 2(b). There the continuous system is described by discrete compartments. The membrane in the junction has a specific capacitance c_{JM} and a specific conductance g_{JM} with a resting voltage V_{JR}. The specific capacitance of the silicon dioxide on the gate is c_{JG}. The core is described by a sheet resistance $r_J=\rho_J/d$ which is determined by the distance d of membrane and chip, and by the specific conductance of the electrolyte ρ_J in the junction. The parameters c_{JM}, g_{JM}, c_{JG}, r_J, and V_{JR} may depend on the position. An electrical stimulation of the neuron gives rise to a current through the membrane in the junction: It spreads along the core to the bulk electrolyte and also through the lower coat to the silicon. As a result, a voltage profile $V_J(x,y,t)$ is built up in the junction which depends on the space coordinates x, y, and the time t.

This ''sandwich cable'' has two pecularities as compared to a common cable: (i) The core-coat conductor is two dimensional. (ii) The cable is stimulated through the coat with the periphery of the core kept on constant potential.

Cable equation. An equation for the dynamics of the voltage $V_J(x,y,t)$ is obtained by applying Kirchhoffs' law and Ohm's law to each infinitesimal area element of the sandwich cable. Taking into account the capacitive and ohmic currents through the membrane, the capacitive current through the silicon dioxide and the ohmic current along the cleft we obtain

$$(c_{JM}+c_{JG})\,\frac{\partial V_J}{\partial t}+g_{JM}V_J-\nabla\left(\frac{1}{r_j}\,\nabla V_J\right)$$

$$=c_{JM}\,\frac{\partial V_M}{\partial t}+g_{JM}(V_M-V_{JR}). \quad (4)$$

The left hand side has the typical structure of a two-dimensional cable equation [10–12]. The lateral stimulation by a voltage $V_M(t)$ is expressed by the right hand side. If we superpose an ac voltage $\underline{V}_M(\omega)$ to a dc voltage, we obtain for the profile of the complex ac voltage $\underline{V}_J(x,y,\omega)$ in the junction

$$(g_{JM}+i\omega c_{JM}+i\omega c_{JG})\underline{V}_J-\nabla\left(\frac{1}{r_j}\,\nabla\underline{V}_j\right)$$

$$=(g_{JM}+i\omega c_{JM})\underline{V}_M. \quad (5)$$

Plate-contact model. We consider a circular junction of radius a_J which is homogeneous with constant values of g_{JM}, c_{JM}, c_{JG}, and r_J. The profile of the ac voltage $\underline{V}_J(a,\omega)$ along the radial coordinate a for a periodic stimulation $\underline{V}_M(\omega)$ is given by Eq. (6) with the length constant λ and the time constant τ of the cable and with the time constant τ_{JM} of the membrane:

$$\left[\lambda^2\,\frac{d^2}{da^2}+\frac{\lambda^2}{a}\,\frac{d}{da}-(1+i\omega\tau)\right]\underline{V}_J(a)=-(1+i\omega\tau_{JM})\underline{V}_M,$$

$$\lambda^2=\frac{1}{g_{JM}r_J},\quad \tau=\frac{c_{JM}+c_{JG}}{g_{JM}},\quad \tau_{JM}=\frac{c_{JM}}{g_{JM}}. \quad (6)$$

We solve Eq. (6) with the periphery kept on ground potential $\underline{V}_J(\omega,a_J)=0$. The transfer function $\underline{h}(\omega,a)=\underline{V}_J(\omega,a)/\underline{V}_M(\omega)$ is given by Eq. (7) in terms of the modified Bessel function of order zero I_0 with the complex damping constant γ_ω.

$$\underline{h}(\omega,a)=\frac{1+i\omega\tau_{JM}}{1+i\omega\tau}\left[1-\frac{I_0(\gamma_\omega a)}{I_0(\gamma_\omega a_J)}\right],$$

$$\gamma_\omega^2=\frac{1+i\omega\tau}{\lambda^2}. \quad (7)$$

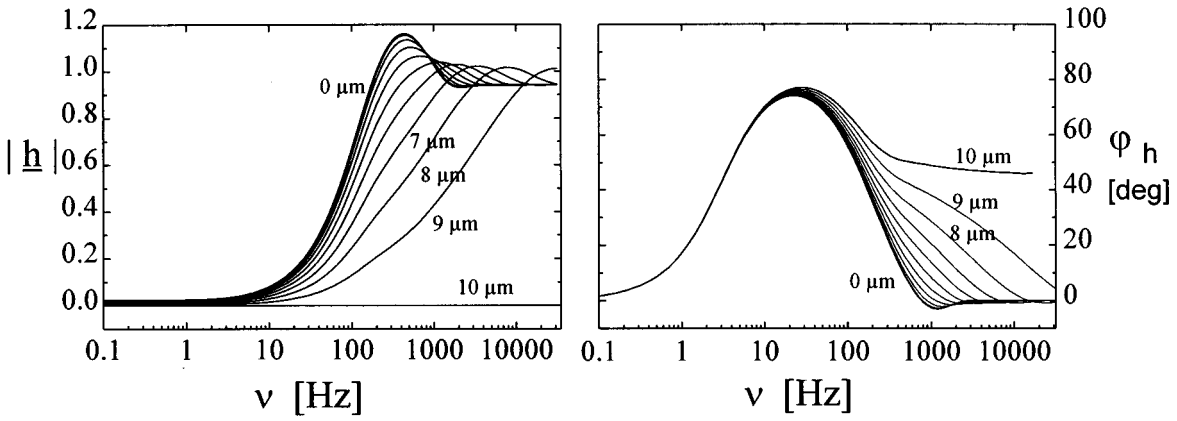

FIG. 3. Theoretical transfer function $\underline{h}=\underline{V}_J/\underline{V}_M$ vs the frequency $\nu=\omega/2\pi$ at different positions along the radius a of a circular homogeneous contact with a radius $a_J=10$ μm. Left: amplitude $|\underline{h}|$. Right: phase φ_h. The parameters are $c_{JM}=5$ μF/cm^2, $g_{JM}=0.1$ mS/cm^2, $c_{JG}=0.3$ μF/cm^2, and $r_J=1$ GΩ.

In the limit of high frequency the second factor of Eq. (7) equals one. The transfer becomes independent of the position and is controlled by the capacitive voltage division in the upper and lower coat according to

$$h_\infty=\frac{\tau_{JM}}{\tau}=\frac{c_{JM}}{c_{JM}+c_{JG}}. \tag{8}$$

In the limit of low frequency the first factor of Eq. (8) equals one. The transfer profile is given by Eq. (9). It has the shape of a cupola. For a cable with little damping, i.e., with a large length constant the cupola is very flat;

$$h_0=1-\frac{I_0(a/\lambda)}{I_0(a_J/\lambda)}. \tag{9}$$

As an example we compute a junction of radius $a_J=10$ μm and width $d=1$ nm. At a specific resistance $\rho_J=100$ Ω cm the sheet resistance is $r_J=1$ GΩ. We choose a capacitance $c_{JM}=5$ μF/cm^2 and a conductance $g_{JM}=0.1$ mS/cm^2 of the membrane and a capacitance $c_{JG}=0.3$ μF/cm^2 of the silicon dioxide. The time and length constant are then $\tau=53$ ms and $\lambda=31.6$ μm. The time constant of the membrane is $\tau_{JM}=50$ ms. The spectra of amplitude and phase are plotted in Fig. 3 versus the frequency $\nu=\omega/2\pi$ for various positions a in the junction.

At low frequency the amplitude is controlled by the ohmic resistances. The voltage profile arises from the centrifugal flow of the current entering through the membrane. In our example the response is small as the length constant is much larger than the radius of the junction. The phase increases around 3 Hz. This transition is given by the time constant of the membrane, i.e., by the condition $\omega\tau_{JM}=1$. There the stimulation changes from Ohmic to capacitive dominance. This phase change occurs all over the plate, there is no phase difference within the junction. The amplitude starts to increase when the impedance of the coat drops at high frequency such that the resistance of the core becomes significant. A characteristic frequency is defined by

$$\omega(c_{JM}+c_{JG})a_J^2r_j=1. \tag{10}$$

There the imaginary component in the argument of the Bessel function becomes significant. With $(c_{JM}+c_{JG})a_J^2r_J=5.3$ ms we expect an enhanced transfer at about 30 Hz as it occurs in the center of the junction (Fig. 3). The enhancement of the amplitude is connected with a drop of the phase. This second transition depends on the position as illustrated in Fig. 3. As a result there are phase shifts along the junction. In a certain range of frequency centripedal currents occur which may enhance the local response in the junction. The local transfer function is then above one as seen in Fig. 3. At a very high frequency the transfer is controlled by the capacitances of the coats according to Eq. (8) with $h_\infty=0.94$. There the phase is zero again.

Averaged plate. A transistor probes the voltage $\underline{V}_J(x,y,\omega)$ at a defined location in the junction if its size is small in comparison to the length constant of the junction. If the transistor channel is short but wide, different components of the source-drain current are modulated by different voltages. If the channel is long, the modulation of the source-drain current may be a complicated function of the voltage profile on the gate. We consider here only a simple case: We assume that the source-drain current is modulated by an average over the total adhesion region with equal weight of each area element. The average transfer in a homogeneous circular junction of radius a_J is

$$\underline{\tilde{h}}(\omega,a_J)=\frac{1+i\omega\tau_{JM}}{1+i\omega\tau}\left[1-\frac{2\pi\int_0^{a_J}I_0(\gamma_\omega a)a\,da}{\pi a_J^2I_0(\gamma_\omega a_J)}\right]. \tag{11}$$

The integral is evaluated numerically using analytical expansions of the Bessel function. The result is shown in Fig. 4(a). The parameters are chosen as above. The phase increases again around 3 Hz. The amplitude increases around 30 Hz with a tail extending to higher frequencies. The dominating part is due to the central region of the junction, the tail to the periphery. The overshooting of the amplitude disappears. For comparison a set of junctions is computed with sheet resistances $r_J=1$ MΩ–10 GΩ. An enhanced seal resistance gives rise to a better transfer at low frequency and shifts the increase of the amplitude to lower frequency. The

increase of the phase is not affected as it depends on the time constant of the membrane alone.

Point-contact model. Usually we do not know the shape of the junction nor the position of the transistor in the junction. Thus we are not able to apply a detailed structural model of the junction. To plan and to evaluate experiments it is useful to introduce the concept of a ''point-contact model'' as illustrated in Fig. 2(c). The membrane is described by a global capacitance C_{JM} and a global resistance R_{JM}, the silicon dioxide by a global capacitance C_{JG} and the core by a characteristic resistance R_J.

The transfer function $\underline{h}(\omega)=\underline{V}_j(\omega)/\underline{V}_M(\omega)$ is obtained again from Kirchhoff's law. It depends on three parameters, the transfer h_0 at vanishing frequency, the time constant τ_{JM} of the membrane and a time constant τ_J of the junction as

$$\underline{h}(\omega)=\frac{1+i\omega\tau_{JM}}{1+i\omega\tau_J}\,h_0, \tag{12a}$$

$$h_0=\frac{R_J}{R_J+R_{JM}}, \tag{12b}$$

$$\tau_{JM}=R_{JM}C_{JM}, \tag{12c}$$

$$\tau_J=\frac{C_{JM}+C_{JG}}{R_{JM}^{-1}+R_J^{-1}}\approx R_J(C_{JM}+C_{JG})\approx R_JC_{JM}. \tag{12d}$$

The approximations of τ_J hold in the case of a high resistance of the membrane and of a small capacitance of the gate oxide, respectively. We note that the transfer at infinite frequency may be expressed by the three parameters as

$$h_\infty=\frac{C_{JM}}{C_{JM}+C_{JG}}=\frac{\tau_{JM}}{\tau_J}\,h_0. \tag{13}$$

At very low and at very high frequency the transfer is governed by the resistances and by the capacitances of the circuit, respectively. In both limits the phase is zero. At an intermediate frequency with $\omega\tau_{JM}\gg 1$ and $\omega\tau_J\ll 1$ we may use Eq. (14) as an approximation of Eq. (12). In that frequency range the phase is 90°:

$$\underline{h}(\omega)\approx i\omega\tau_{JM}h_0. \tag{14}$$

In general it is convenient to express the transfer function by its amplitude $|\underline{h}|$ and its phase φ_h according to Eqs. (15) and (16)

$$|\underline{h}|^2=\frac{1}{1+(\omega\tau_J)^2}\,h_0^2+\frac{(\omega\tau_J)^2}{1+(\omega\tau_J)^2}\,h_\infty^2, \tag{15}$$

$$\tan\varphi_h=\frac{1}{1/\omega\tau_{JM}+\omega\tau_J}\left(1-\frac{\tau_J}{\tau_{JM}}\right). \tag{16}$$

We see from Eq. (15) that the time constant τ_J determines the transition of the amplitude from the low-frequency limit to the high-frequency limit. Equation (16) shows that the phase vanishes at very high and at very low frequencies.

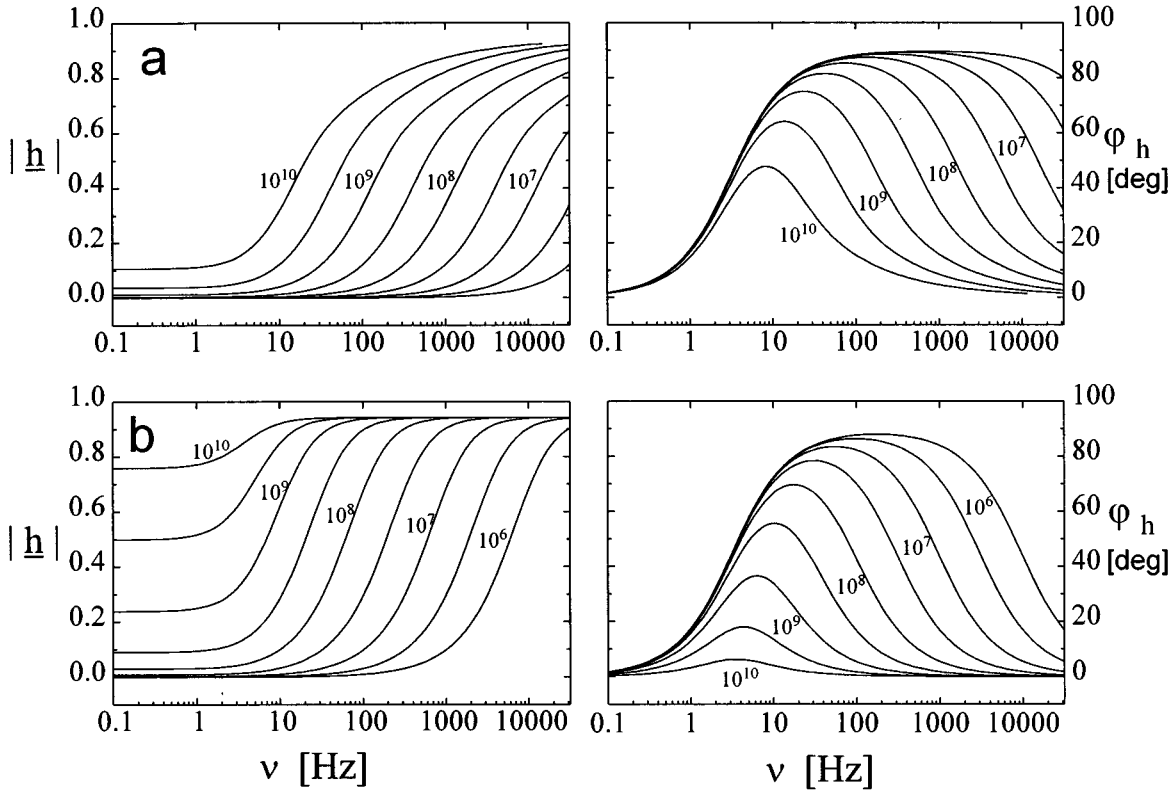

FIG. 4. Theoretical transfer functions $\underline{h}=\underline{V}_J/\underline{V}_M$. (a) Averaged plate model with amplitude $|\underline{h}|$ on the left and phase φ_h on the right. The parameters are $c_{JM}=5\ \mu$F/cm^2, $g_{JM}=0.1$ mS/cm^2, and $c_{JS}=0.3\ \mu$F/cm^2 with a radius $a_J=10\ \mu$m. The sheet resistances are $r_J=10^6$–10^{10} Ω as indicated. (b) Point-contact model with amplitude $|\underline{h}|$ on the left and phase φ_h on the right. The parameters are $C_{JM}=15.7$ pF, $R_{JM}=3.2$ GΩ, $C_{JG}=0.94$ pF, and $R_J=10^6$–10^{10} Ω as indicated.

Point contact and plate contact. To better understand the nature of the point-contact model we evaluate its elements C_{JM}, R_{JM}, C_{JG}, and R_J for a plate contact of radius a_J with the parameters c_{JM}, g_{JM}, c_{JG}, and r_J. We express the capacitance C_{JM} and the resistance R_{JM} by the specific capacitance and conductance of the membrane and by the total contact area as $C_{JM}=c_{JM}a_J^2\pi$ and $R_{JM}=(g_{JM}a_J^2\pi)^{-1}$ and use a similar relation for the capacitance of the gate as $C_{JG}=c_{JG}a_J^2\pi$. To obtain a global seal resistance R_J we define a representative location within the junction. The average radius in each segment of the plate is $(2/3)a_J$. We assume that the contact is concentrated in a narrow ring of that radius. This location is sealed from the periphery by a ring-shaped sheet. The length of that resistor is $(1/3)a_J$ and its average width is $2\pi(5/6)a_J$. As a result we obtain for the seal resistance of the representative location

$$R_J=\frac{r_J}{5\pi}. \tag{17}$$

It is notable that the radius of the junction cancels in this expression. For the plate contact considered above with $a_J=10$ μm, $c_{JM}=5$ μF/cm^2, $g_{JM}=0.1$ mS/cm^2, $c_{JG}=0.3$ μF/cm^2, and $r_J=1$ GΩ we obtain as parameters of the point-contact model $C_{JM}=15.7$ pF, $R_{JM}=3.2$ GΩ, $C_{JG}=0.94$ pF, and $R_J=63.7$ MΩ.

A set of transfer functions of the point-contact model is shown in Fig. 4(b) for $C_{JM}=15.7$ pF, $R_{JM}=3.2$ GΩ, $C_{JG}=0.94$ pF, and seal resistances $R_J=1$ MΩ–10 GΩ. The figure illustrates the transition from a low-frequency limit to a high-frequency limit. A high seal resistance enhances the amplitude at low frequency and shifts the transition at $\omega\tau_J=1$ to lower frequency. The increase of the phase occurs at $\omega\tau_{JM}=1$. Apparently the changes of amplitude and phase are rather similar to those of the plate-contact model [Fig. 4(a)]. The spectra of the plate contact with a sheet resistance r_J correspond well to those of the point contact with a seal resistance $R_J=r_J/5\pi$.

III. MATERIALS AND METHODS

In this section we describe the fabrication of the transistors, the preparation of neurons, and the assembly of neuron transistors. Then we discuss the methods of measurement—of the impedance of the attached neuron and of the voltage transfer from the neuron to the gate of the transistor.

Transistor. Chips of a size 30 mm×10 mm were cut from *n*-type silicon wafers with a 100 surface (Wacker-Chemie, Burghausen). After cleaning by the standard RCA (Radio Corporation of America) procedure we oxidized them in wet oxygen at 1000 °C. Openings for sources and drains were structured by photolithography and etched with ammonium fluoride solution (AF 87.5–12.5, Merck, Darmstadt). We arranged two times 16 transistors on the chip, each set in a quadratic array with a distance of 300 μm between the transistors [Fig. 5(b)]. The transistors had individual drains and shared a common source. Doping was achieved by deposition of a boron glass by evaporation from planar sources of boron nitride (Sohio Engineered Materials, New York) at 900 °C and a driving-in process at 1100 °C for 2 h. The boron glass and the mask oxide were removed. The width of source and drain was about 50 μm, the length of the channel was 6 μm. A field oxide (1 μm thick) was grown at 1000 °C. Around each channel we etched an area of 30 μm diameter in the field oxide. This region was covered by a thin gate oxide with a thickness of 12 nm (dry oxidation at 1000 °C). The *p*-doped lanes of the drains and the source lead radially from the transistors to contact pads on a circle of 6 mm, which were opened in a last step and covered by sintered aluminium. Finally two chips of a size 10 mm×10 mm with a single array of transistors were cut and stuck on a printed plate (50 mm×70 mm) with copper leads [Fig. 5(a)]. Drains and sources were connected to the plate by aluminium wire bonding. Finally a circular chamber was attached which shields the bond contacts from the bath solution. The chamber was made of Plexiglas. It was stuck onto the silicon with a silicone glue and stabilized by a ring of Plexiglas. Within the chamber only silicon dioxide was exposed.

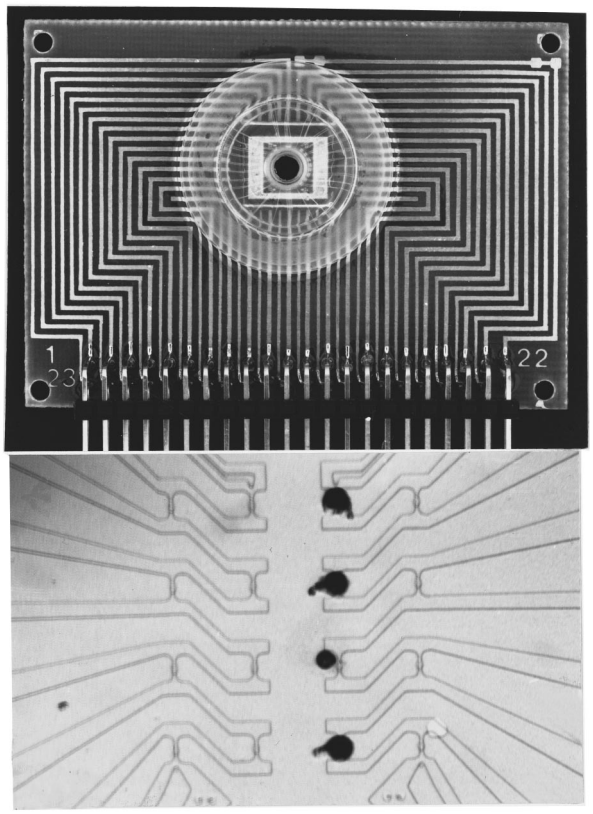

FIG. 5. Neurochip. (a) A chip of the size 10 mm×10 mm is wire bonded to a plate with copper leads. A circular chamber of Plexiglas is attached to contain the electrolyte. (b) Central region of the chip. Sixteen transistors are arranged as a 4×4 array. The distance of the gates is about 300 μm. Each transistor has its own drain pointing to the left or right. The common source is in the center. Retzius cells are attached to the metal-free gates of several transistors. Their diameter is about 60 μm.

We checked each transistor by measuring the output and transfer characteristics. We varied the potential of bulk silicon with respect to the electrolyte which was kept on ground potential. The source-drain current was measured for different values of the drain potential with the source kept on bulk potential. From this set of data we defined a working point. We usually chose a voltage $V_{ES}=-3$ V between electrolyte

and bulk silicon and a voltage $V_{DS}=-2$ V between drain and source. The source-drain current was then around 100–150 μA. We calibrated each transistor at its working point by superposing ac voltages to the bath potential and measured the modulation of the source drain current.

The transistor arrays could be reused many times and still worked after several months of measurement. The source-drain current at the working point differed somewhat from measurement to measurement. This effect did not affect the final result as the dc component of the source-drain current was subtracted. No corrosion was visible even with gate oxides as thin as 10 nm with a voltage up to +5 V applied to the silicon. We think that the silicon dioxide is stable under these conditions because the positive potential prevents the invasion of cations into the oxide and into the silicon surface and because any holes which might occur would be sealed by anodic oxidation.

Neurons. Five to ten centimeter long leeches (*Hirudo medicinalis*) were maintained at 4 °C in water. The segmental ganglia were dissected and pinned on a Sylgard coated dish containing Leibowitz L-15 medium (Gibco, Eggenstein) supplemented with 30 μg/ml gentamycinsulfate (Sigma), 5 mg/ml Glucose and 2% foetal calf serum (Gibco) [13]. The capsules around the ganglia were incubated in dispase and collagenase (Boehringer, Mannheim) (2 mg/ml L15 medium) for 1 h. The Retzius cells were removed by aspiration into a fire-polished pipette and washed in several drops of medium [13]. About 20 to 30 Retzius cells were isolated from each leech. Due to the relatively large size (diameter 50–80 μm) these neurons are easy to handle. After dissociation, the neurons were kept in a supplemented L-15 medium at 21 °C for 5 to 24 h. Before attachment to a chip they were treated with collagenase and dispase for half an hour to clean the membrane from connective tissue. Finally they were transferred to serumfree L-15 medium.

We used some of the Retzius cells to determine the electrical parameters of their membrane. We found a considerable variance. The time constants were $\tau_M=10$–50 ms, the capacitances varied within $C_M=0.5$–3 nF, and the resistances within $R_M=5$–50 MΩ when the neuron was kept at a voltage of $V_M=-40$ to -60 mV. From an estimate of the cell surface we obtained a specific capacitance of the membrane of about $c_M=5$ μF/cm^2 and a specific conductance about $g_M=0.25$ mS/cm^2. The conductance is in a range typical for neurons in their resting state (e.g., 0.67 mS/cm^2 in the squid axon [9]). The capacitance is much higher than 1 μF/cm^2 as assigned usually to plasma membranes. The origin of this enhancement is unknown. It may be due microfolding of the membrane.

Assembly. The surface of the chip in a chamber was cleaned by hot (80 °C) basic peroxide (30% hydrogen peroxide, 25% ammonia and water at a volume ratio 1:1:5) for 1–3 min wiping with kimwipe paper. After careful rinsing with water, a drop of an aqueous solution of poly-L-lysine (1 mg/ml, MW 15 000–30 000 Sigma, Germany) was applied to each gate area and dried. The chamber was filled with serumfree L-15 medium. Retzius cells were transferred within 5 min to each gate under visual control in a stereomicroscope (Wild M10, Heerbrugg, Switzerland) using a glass pipette with an opening of 100 μm. The cells adhered immediately after touching the surface.

Patch clamp. A neuron on a gate was contacted with a fire-polished patch pipette (opening 3–4 μm) using a micromanipulator. The pipette was filled with 140 m*M* KCl, 1.5 m*M* $MgCl_2$, 10 m*M* EGTA [ethylene glycol-bis (β-eminoethylether) N,N, $N_1^1N^1$-tetraacetic acid] and 10 m*M* HEPES [(N-[2-hydroxyethyl]piperazine-N^1-[2-ethanesulfonic acid] at *p*H 7.4. The pipette was fused with the cell membrane by suction and sometimes by a short electrical pulse [14]. The seal resistance was better than 300 MΩ. The neurons were kept at a voltage of -40 to -60 mV to prevent spontaneous firing.

We used a single-electrode patch-clamp amplifier (npi-electronic, Tamm, Germany). A command signal of variable frequency was applied to the amplifier. The actual ac modulation of the voltage $\underline{V}_p$ in the headstage of the pipette could differ from the command signal due to the feedback circuit of the amplifier. We measured the actual modulation $\underline{V}_p$ by a two-phase lock-in amplifier (Stanford Instruments, Stanford). In addition we measured the ac modulation of the current $\underline{I}_p$ through the pipette using a second two-phase lock-in amplifier. We did not use any amplifier compensation. Thus the ac modulation $\underline{V}_M$ of the voltage in the neuron was not clamped.

Impedance. We measured the spectrum of the complex impedance $\underline{Z}=\underline{V}_p/\underline{I}_p$ of a patched neuron on the chip for two reasons: (i) We determined a representative circuit of the patched neuron which was used to evaluate the actual intracellular voltage $\underline{V}_M$. (ii) We obtained information about the electrical properties of the attached neuron.

The complete representative circuit of a patched neuron on a chip is shown in Fig. 6(a). The pipette is described by an access resistance R_A and by a stray capacitance C_{ST}. For reasons discussed later we introduce an access capacitance C_A. The free neuron membrane has a capacitance C_{FM} and a resistance R_{FM}. The junction itself is described by the point-contact model.

To evaluate the impedance spectra we replace the complete circuit by the simplified circuit of Fig. 6(b). The free membrane and the junction together are described by an effective capacitance $\tilde{C}_M$ and an effective resistance $\tilde{R}_M$, the pipette by an effective access resistance $\tilde{R}_A$ and an effective stray capacitance $\tilde{C}_{ST}$. The impedance is

$$\underline{Z}(\omega)=\frac{\underline{V}_P(\omega)}{\underline{I}_P(\omega)}=\left[\frac{1}{\tilde{R}_A+1/(\tilde{R}_M^{-1}+i\omega\tilde{C}_M)}+i\omega\tilde{C}_{ST}\right]^{-1}. \tag{18}$$

The amplitude and the phase of the experimental data were fitted according to Eq. (18) using a Levenberg-Marquardt algorithm. We estimated that the accuracy of the parameters $\tilde{C}_M$ and $\tilde{R}_M$ is better than 6% and of $\tilde{R}_A$ and $\tilde{C}_{ST}$ better than 10%.

Transfer function. The experimental transfer function is the ratio of the effective voltage on the gate $\underline{V}_J$ and of the voltage in the neuron $\underline{V}_M$

$$\underline{h}(\omega)=\frac{\underline{V}_J}{\underline{V}_M}. \tag{19}$$

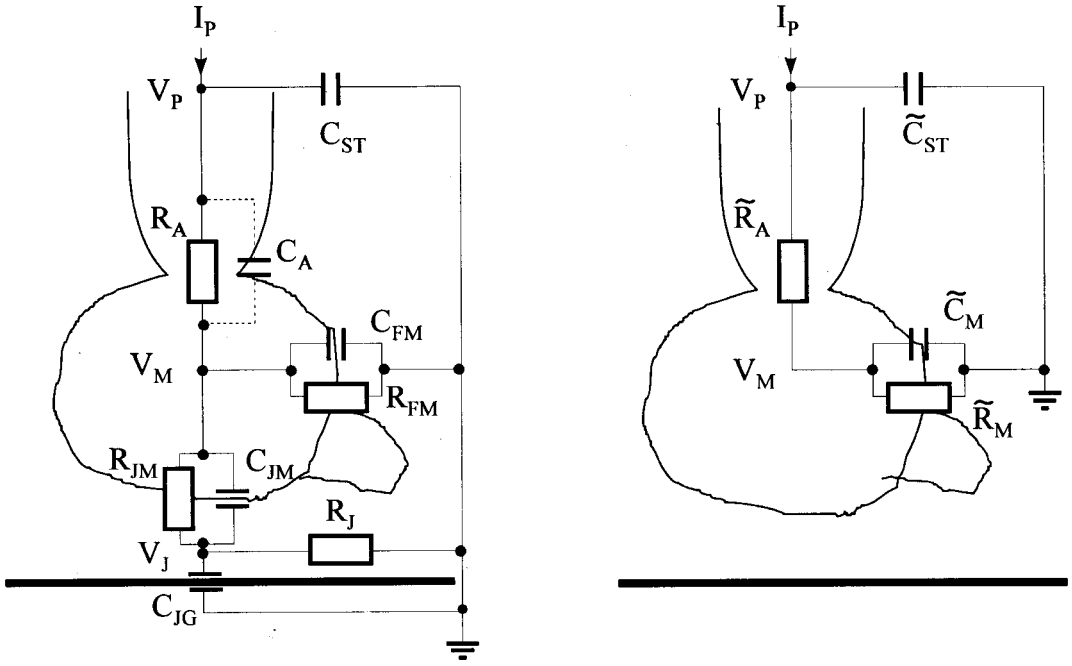

FIG. 6. Circuit of a neuron on a chip with fused patch pipette. (a) Complete circuit. The pipette is described by an access resistance R_A, an access capacitance C_A, and a stray capacitance C_{ST}. The free membrane is described by the capacitance C_{FM} and the resistance R_{FM}. The junction itself is represented by the point-contact model with a resistance R_{JM} and a capacitance C_{JM} of the membrane, a capacitance C_{JG} of the silicon dioxide and a seal resistance R_J. (b) Reduced circuit. The whole neuron with the junction is described by an effective membrane capacitance $\tilde{C}_M$ and an effective membrane resistance $\tilde{R}_M$. The pipette is given by an effective access resistance $\tilde{R}_A$ and an effective stray capacitance $\tilde{C}_{ST}$.

The effective voltage in the junction $\underline{V}_J(\omega)$ is obtained from the modulation of the source-drain current. The modulation $\underline{I}_D(\omega)$ is observed by a two-phase lock-in amplifier when the pipette is stimulated with $\underline{V}_P(\omega)$. We transform the result into a modulation of the voltage in the junction $\underline{V}_J(\omega)$. The calibration is made without neuron by superposing an ac signal to the electrolyte potential and observing the source-drain current. Such a calibration implies that an attached neuron does not affect the electrical properties of the transistor.

The unknown voltage $\underline{V}_M(\omega)$ in the neuron is computed from the voltage in the headstage $\underline{V}_P(\omega)$ using the circuit as determined by the impedance. We obtain

$$\frac{\underline{V}_M(\omega)}{\underline{V}_P(\omega)} = \frac{1/(\tilde{R}_M^{-1} + i\omega\tilde{C}_M)}{1/(\tilde{R}_M^{-1} + i\omega\tilde{C}_M) + R_A/(1 + i\omega R_A C_A)}. \quad (20)$$

We have to consider here explicitly the effective access capacitance C_A which affects the voltage drop in the pipette. We use two kinds of evaluation: (i) In a first approach we determine the intracellular voltage with $C_A = 0$. That is, we assume that the voltage drop in the pipette is Ohmic. (ii) In a second approach we estimate an access capacitance $C_A \neq 0$ on the basis of the experimental stray capacitance $\tilde{C}_{ST}$. The necessity for the second procedure is discussed below. In both cases we use the approximation $R_A \approx \tilde{R}_A$.

IV. RESULTS AND DISCUSSION

First we consider the impedance of neurons attached to transistors. On this basis we determine the frequency-dependent voltage transfer from the neurons to the transistors. We evaluate the results in terms of the sandwich cable using the point-contact model and the plate-contact model. Finally we use the experimental ac-transfer functions to compute the signal transfer of an action potential. The three neuron-silicon junctions presented here are representative examples of many experiments. The features of junctions 1 and 3 are observed frequently, whereas a junction such as No. 2 is rare.

Impedance. The impedance spectra of three neurons attached to transistors are shown in Fig. 7. We discuss them in terms of the representative circuit of Fig. 6(b). At low frequency the amplitude is given by the membrane resistance $\tilde{R}_M$. With increasing frequency the parallel capacitance of the membrane $\tilde{C}_M$ starts to contribute and the access resistance $\tilde{R}_A$ in series dominates. Finally the stray capacitance $\tilde{C}_{ST}$ becomes effective. As a result the amplitude drops in two steps with increasing frequency and the phase drops, increases and drops again. There is an apparent difference in the three junctions: The primary drop of the amplitude and the dip in the phase is shifted to a higher frequency in the junctions 1 to 3.

A fit of the data is drawn in Fig. 7 with the parameters summarized in Table I. We obtain fairly constant values of the access resistance and of the stray capacitance which are around $\tilde{R}_A = 1$ MΩ and $\tilde{C}_{ST} = 20$ pF. Most significant is the change of the time constant $\tilde{\tau}_M = \tilde{R}_M \tilde{C}_M$. The value of $\tilde{\tau}_M = 17.7$ ms in neuron 1 is typical for a free Retzius cell after patching, a value such as $\tilde{\tau}_M = 0.88$ ms, in neuron 3, however, is significantly lower. The change suggests an enhanced conductance in the attached part of the membrane.

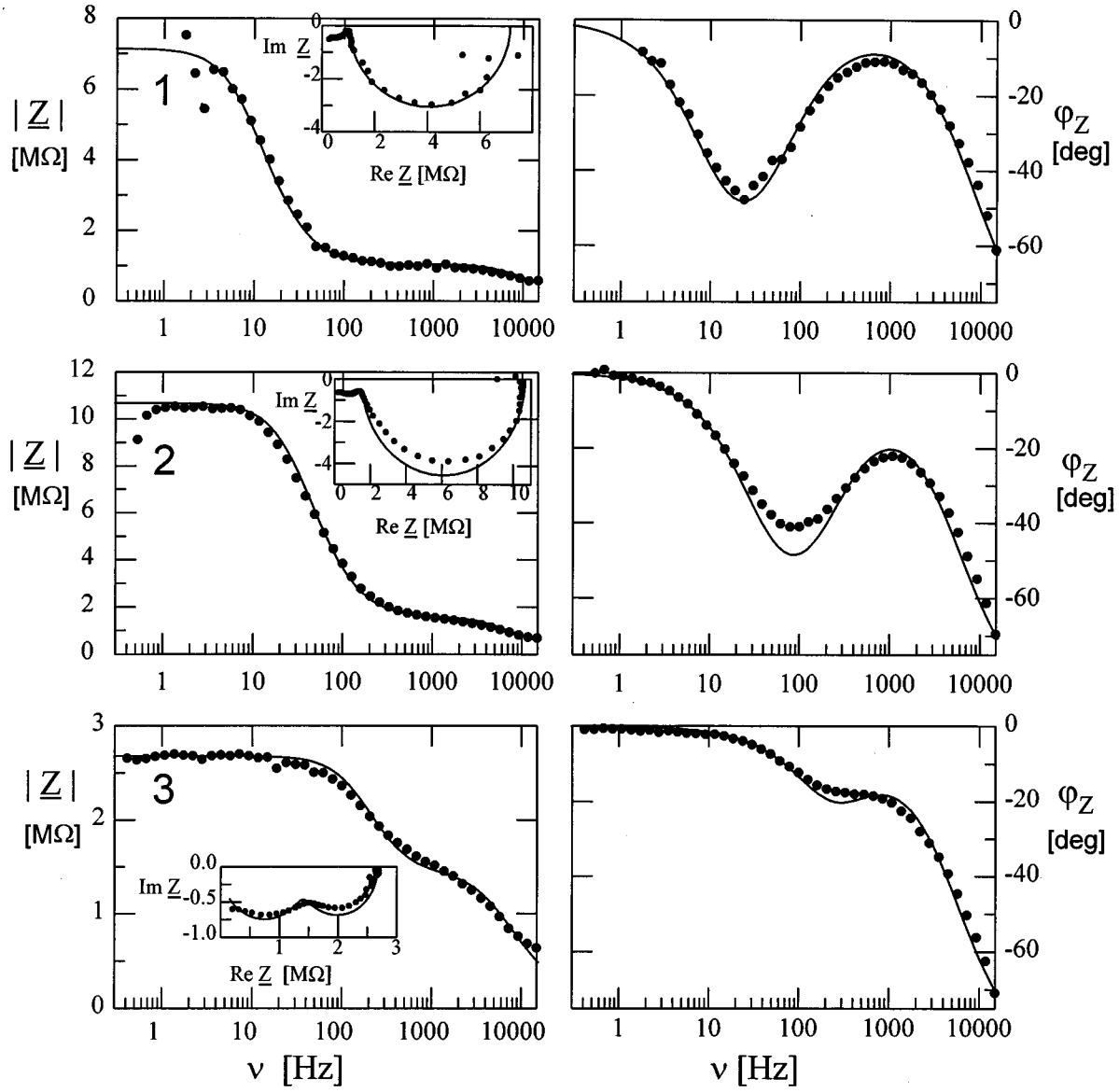

FIG. 7. Impedance $\underline{Z}=\underline{V}_P/\underline{I}_P$ of the three neuron transistors 1, 2, and 3. Bode plot with amplitude $|\underline{Z}|$ (left) and phase φ_Z (right) vs the frequency ν. Nyquist plots Im$\underline{Z}$ versus Re $\underline{Z}$ are shown as inserts. The drop of the amplitude and the dip of the phase are shifted to higher frequencies in junctions 1 to 3. The data are fitted according to the circuit of Fig. 6(b). The parameters are given in Table I.

There is, however, a problem in comparing different junctions because of the variability of the Retzius cells themselves. We assign the differences in the capacitance in Table I to a different size of the neurons. We scale then the resistance $\widetilde{R}_M$ to a capacitance of $\widetilde{C}_M=0.5$ nF. Table I shows that the standardized resistance $\widetilde{R}'_M$ drops from 35.4 MΩ to 9.6 MΩ and 1.74 MΩ from junction 1 to 3.

Transfer function. The spectral transfer $\underline{h}(\omega)=\underline{V}_J/\underline{V}_M$ of the three neuron transistors is shown in Fig. 8. The membrane voltage $\underline{V}_M$ was determined from the voltage $\underline{V}_P$ ap-

TABLE I. Impedance measurement. Parameters of three neuron-silicon junctions as obtained from impedance measurements using the circuit of Fig. 6(b): Effective time constant of the membrane $\widetilde{\tau}_M$, effective capacitance $\widetilde{C}_M$, and resistance $\widetilde{R}_M$ of the membrane, effective access resistance $\widetilde{R}_A$ and effective stray capacitance $\widetilde{C}_{ST}$ of the pipette. In addition, the normalized resistance $\widetilde{R}'_M$ of the membrane is given which is scaled to a capacitance of $\widetilde{C}_M=0.5$ nF/cm^2.

Junction	$\widetilde{\tau}_M$ (ms)	$\widetilde{C}_M$ (nF)	$\widetilde{R}_M$ (MΩ)	$\widetilde{R}'_M$ (MΩ)	$\widetilde{R}_A$ (MΩ)	$\widetilde{C}_{ST}$ (pF)
1	17.7	2.9	6.1	35.4	1.05	18.3
2	4.8	0.53	9.1	9.6	1.56	17.7
3	0.88	0.69	1.28	1.75	1.42	20.3

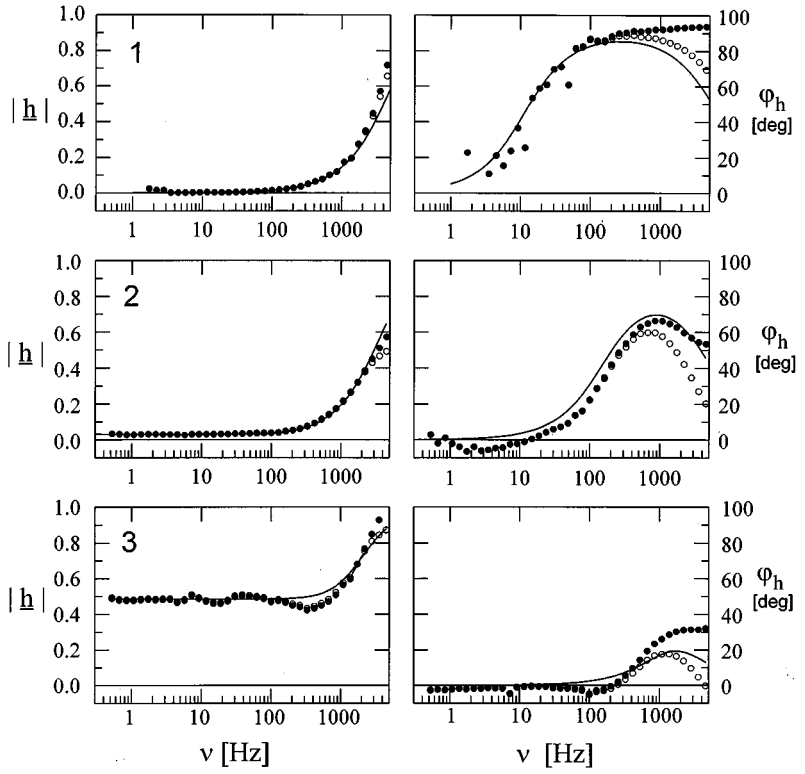

FIG. 8. Experimental transfer functions $\underline{h}=\underline{V}_J/\underline{V}_M$ of the three neuron transistors 1, 2, and 3. Amplitude $|\underline{h}|$ (left) and phase φ_h (right) vs the frequency ν. Two sets of data are shown as obtained with a different evaluation of the intracellular voltage $\underline{V}_M$. The black dots are determined without access capacitance $C_A=0$. The white circles are obtained with an access capacitance $C_A=C_{ST}-3$ pF. The curves are computed with the point-contact model. The parameters are obtained from a fit of the model to the amplitudes using the double-logarithmic plot of Fig. 9.

plied to the pipette according to Eq. (20) with the parameters $\tilde{R}_M, \tilde{C}_M, R_A \approx \tilde{R}_A$ taken from the impedance measurement. An access capacitance C_A was not taken into account. First we discuss the spectra qualitatively, then we evaluate the amplitudes $|\underline{h}|$ in terms of the point-contact model. In a next step we consider the phases φ_h taking into account an access capacitance C_A. Finally we consider the plate-contact model.

At low frequency the amplitude in junction 1 is below 0.01. The phase is small there with a large error of the measurement due to the small amplitude. The phase increases around 10 Hz up to 90°, whereas the amplitude grows in the range of 1000 Hz. In junction 3 the amplitude is rather high—about 0.5—already at the lowest frequency. Around 1000 Hz it increases up to 0.9. A modest increase of the phase up to 30° occurs above 100 Hz. The transfer function of junction 2 is between that of junction 1 and junction 3: The phase increases here around 100 Hz. The amplitude at low frequency is small but with about 0.03 distinctly higher than in junction 1. The enhancement of the amplitude occurs at a similar frequency in all three junctions. The crucial difference in the junctions 1, 2, and 3 is the enhanced coupling at low frequency and the displacement of the phase shift to higher frequency.

Amplitude. We fit the point-contact model to the amplitudes alone according to Eq. (15). In a range well below the transition frequency $\omega\tau_J \ll 1$ we may write

$$\log_{10}|\underline{h}| = \log_{10}|h_0| + \tfrac{1}{2}\log_{10}(1+\omega^2\tau_{JM}^2). \qquad (21)$$

Surprisingly the onset of the transition to the limit of high frequency depends on the time constant of the membrane τ_{JM} not on the time constant τ_J. In a double-logarithmic diagram the time constant τ_{JM} is defined by the intersection of the low-frequency limit h_0 and of the transition region of slope one.

The experimental data are replotted in Fig. 9. The onset of the transition is seen particularly well for the junction 2. We fit a low-frequency limit $h_0=0.031$ and a time constant $\tau_{JM}=1.0$ ms. In junction 1 the onset is shifted to lower frequency. Due to the small coupling at low frequency the evaluation is less defined. We assign $h_0=0.0017$ and $\tau_{JM}=14$ ms. In junction 3 the onset is shifted to high frequency. The linear part of the transition is hardly visible as the onset is too close to the transition frequency itself. We assign here $h_0=0.48$ and $\tau_{JM}=0.13$ ms.

The fit parameters are summarized in Table II. The amplitude at low frequency h_0 is enhanced and the time constant τ_{JM} is reduced in junction 1 to 3 by orders of magnitude. From Eq. (13) we may evaluate the time constant τ_J if we assume that the transfer at high frequency is constant in

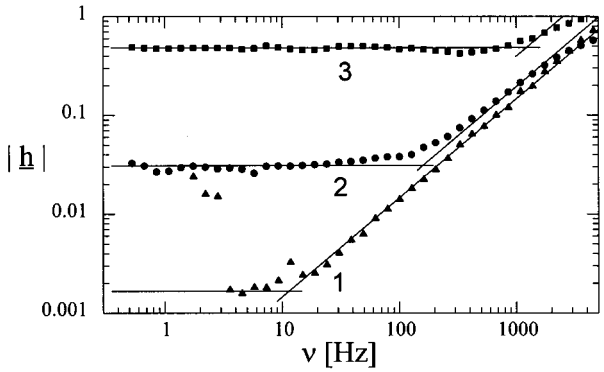

FIG. 9. Experimental amplitude $|\underline{h}|$ of the transfer function vs the frequency ν. Double-logarithmic plot for the junctions 1, 2, and 3. The low frequency limits are fitted by a constant h_0. The onset of the transition to the high frequency limit is fitted by a line of slope one. The time constant τ_{JM} is obtained from the intersection. The parameters h_0 and τ_{JM} are given in Table II.

TABLE II. Transfer function. Parameters of three neuron transistors: Amplitude at low frequency h_0, time constant of the membrane τ_{JM}, time constant of the junction τ_J, resistance of the membrane R_{JM}, seal resistance R_J, specific membrane conductance g_{JM}, averaged length constant λ, sheet resistance r_J, and distance d of membrane and silicon dioxide. The capacitances of the membrane and of the silicon oxide are $C_{JM}=50$ pF and $C_{JG}=3$ pF.

Junction	h_0	τ_{JM} (ms)	τ_J (μs)	R_{JM} (MΩ)	R_J (MΩ)	g_{JM} (mS/cm^2)	λ (μm)	r_J (mΩ)	d (nm)
1	0.0017	14.0	25	280	0.46	0.36	190	7.7	130
2	0.031	1.0	33	20	0.64	5.0	43	10.8	93
3	0.48	0.13	66	2.6	2.45	38.5	8	41.0	24

all junctions, given by the ratio of the specific capacitances $h_\infty=c_{JM}/(c_{JM}+c_{JG})$. With $c_M=5$ μF/cm^2 and $c_{JG}=0.3$ μF/cm^2 we obtain $h_\infty=0.94$ and $\tau_J=25$, 33, 66 μs for the three junctions. The transition frequency differs only little in the three junctions.

The local time constant $\tau_{JM}=14$ ms of the membrane in junction 1 is very close to the effective time constant $\tilde{\tau}_M=17.7$ ms of the whole cell as obtained from the impedance measurement. This coincidence shows that the formation of this junction does not significantly affect the membrane.

On the other hand, the extremely small time constant $\tau_{JM}=0.13$ ms in junction 3 indicates that there the attachment has lowered the membrane resistance by two orders of magnitude. We may relate this result with the small effective time constant $\tilde{\tau}_M=0.88$ ms of the whole neuron as given by the impedance measurement. Let us assume that the junction is formed by an area fraction α of the total cell surface. The effective time constant $\tilde{\tau}_M$ may be expressed by the time constants of the free and attached membrane τ_M and τ_{JM}

$$\frac{1}{\tilde{\tau}_M}=\frac{1-\alpha}{\tau_M}+\frac{\alpha}{\tau_{JM}}. \tag{22}$$

For a time constant of the free membrane in the order of $\tau_M=10$ ms we obtain with $\tilde{\tau}_M=0.88$ ms and $\tau_{JM}=0.13$ ms an area fraction of $\alpha=0.14$. This value is in a reasonable range considering the geometry of attachment.

To determine the four electrical elements of the point-contact model from the three parameters h_0, τ_{JM}, τ_J we have to define the absolute value of one element. Assuming a contact area 1000 μm^2 we obtain a total capacitance $C_{JM}=50$ pF. The capacitance of the silicon dioxide is then $C_{JG}=2$ pF. The resistances of the membrane R_{JM} and of the junction R_J obtained from Eq. (12) are summarized in Table II. The resistance of the junction is in the order of 1 MΩ in all three systems. It is significantly enhanced in junction 3. On the other hand, the resistance of the membrane decreases drastically from junction 1 to 3 with $R_{JM}=280$, 20, 2.6 MΩ.

It is the crucial difference between the different junctions that the resistance of the membrane can differ by orders of magnitude. This effect is correlated with an enhanced resistance of the junction.

Phase. We compute the phases of the junctions according to Eq. (16) using the parameters τ_{JM} and τ_J evaluated from the amplitudes. The result is shown in Fig. 8. The increase of the phase at different frequencies in the three junctions is described well. That is, amplitude and phase are consistent with respect to the time constant of the membrane τ_{JM}. We compute, however, a drop of the phase at higher frequency in the region of the transition defined by $\omega\tau_J=1$. That effect is seen in junction 2, but not in junction 1 and 3 (Fig. 8).

We think that this discrepancy of amplitude spectrum and phase spectrum is due to an additional capacitive pathway from the stimulating pipette into the gate. For example, the voltage in the pipette may couple through the stray capacitance C_{ST} into the bath [Fig. 6(a)]. The signal is not grounded completely at high frequencies: The impedance of the capacitance is low and the resistance of the bath (around 10 kΩ) becomes relevant there. The signal may couple then from the bath into junction. In order to study these effects it would be necessary to vary systematically the experimental setup. Such an investigation was beyond the present paper.

To account for an unspecified capacitive pathway we introduce a formal access capacitance C_A of the pipette [Fig. 6(a)]. This capacitance enhances the signal transfer from the headstage into the cell at high frequency. We have to determine the intracellular voltage V_M according to Eq. (20). We estimate as an upper limit of the access capacitance $C_A=15.3$, 14.7, 17.3 pF for the three junctions. These values are given by the total stray capacitances C_{ST} obtained from the impedances (Table II) diminished by the stray capacitance 3 pF of the headstage. The resulting transfer function is shown in Fig. 8. Apparently the experimental amplitudes change little, even for this extreme case. The experimental phase shifts, however, drop now at high frequency as it is implied in the point-contact model.

Plate-contact model. We try to interpret the data also with the plate-contact model. We use the specific capacitances of membrane $c_{JM}=5$ μF/cm^2 and of silicon dioxide $c_{JG}=0.3$ μF/cm^2 and choose a radius $a_J=18$ μm to obtain an area of 1000 μm^2 as above. The fit parameters are then the specific conductance of the membrane g_{JM} and the sheet resistance r_J.

At first we consider the time constant $\tau_{JM}=c_{JM}/g_{JM}$ which is independent of the size of the junction and on the location of the transistor. We are allowed to take the experimental values as evaluated with the point-contact model (Table II). With $c_{JM}=5$ μF/cm^2 we obtain the conductances $g_{JM}=0.36$, 5.0, 38.5 mS/cm^2 for the three junctions. Even the largest value is within the typical range of a neuron membrane with open ion channels. For example, the conductance of open potassium channels in the squid axon is 36 mS/cm^2 [9].

The amplitude h_0 at low frequency depends on the length constant λ and on the size of the junction according to Eq.

(8). We have to specify also the site of detection. The gate with a length of 6 μm and a width of 30 μm probes a line across a circular junction of 36 μm diameter. Without structural information we consider two limiting cases: (i) The gate is a pointlike detector in the center of the junction. (ii) The gate averages the whole junction homogeneously. That is, we use on one hand Eq. (9) with $a=0$ and on the other hand Eq. (11). We compute h_0 for various length constants and compare the results with the experimental values of Table II. We obtain for each junction optimal length constants for the two limiting cases: (221 μm)/(157 μm) for junction 1, (50.6 μm)/(35.4 μm) for junction 2, and (10.2 μm)/(5.6 μm) for junction 3. The averages of the two cases are $\lambda=190$ μm, 43 μm, and 8 μm for junctions 1, 2, and 3. In junction 1 the length constant is larger than the diameter, in junction 2 it is similar to the diameter, and in junction 3 it is shorter than the diameter.

The sheet resistance is given by $\lambda^2=1/g_{JM}r_J$. From the average length constants and the specific conductances we obtain $r_J=7.7$ MΩ, 10.8 MΩ, 41 MΩ. These values are by a factor of 16.7 larger than the values of R_J in the point-contact model. This ratio is compatible with a ratio $r_J/R_J=5\pi$ according to Eq. (17).

In a last step we determine the distance d of membrane and silicon dioxide from $r_J=\rho_J/d$. We take the specific resistance of bulk electrolyte with $\rho_J=100$ Ω cm. We obtain 130 nm, 93 nm, 24 nm for the three junctions. The width of the sandwich cable is about three orders of magnitude smaller than its diameter. This result justifies the picture of an extended cablelike structure.

Signal transfer. The complex ac-transfer function determines the ac component of an arbitrary time-dependent voltage from a neuron to a transistor. The ac component of the response $V_J(t)$ in the junction is given by a convolution of the intracellular signal $V_M(t)$ with the Fourier transform of the transfer function $\underline{h}(\omega)$. It may be computed by Fourier transformation of the signal, filtering the spectrum with the transfer function and Fourier backtransformation according to Eq. (23)

$$\underline{V}_M(\omega)=\int_{-\infty}^{+\infty} V_M(t)e^{-i\omega t}dt, \tag{23a}$$

$$\underline{V}_J(\omega)=\underline{h}(\omega)\underline{V}_M(\omega), \tag{23b}$$

$$V_J(t)=\frac{1}{2\pi}\int_{-\infty}^{+\infty}\underline{V}_J(\omega)e^{i\omega t}d\omega. \tag{23c}$$

We compute the ac component of the response to an action potential $V_M(t)$ of a Retzius cell. We describe the transfer functions of the junctions 1, 2, and 3 by the point-contact model according to Eq. (12) with the parameters summarized in Table II. The results are shown in Fig. 10.

The ac response of junction 1 to an action potential is biphasic and rather weak with an amplitude of 2 mV. It resembles a weakened first derivative of the stimulus. This feature is due to the fact that the transfer function (Fig. 8) has a low amplitude over wide spectral range. A significant contribution occurs only above 100 Hz where the phase is near 90°. There the transfer function can be approximated by Eq. (14). In fact such a weak biphasic response was observed

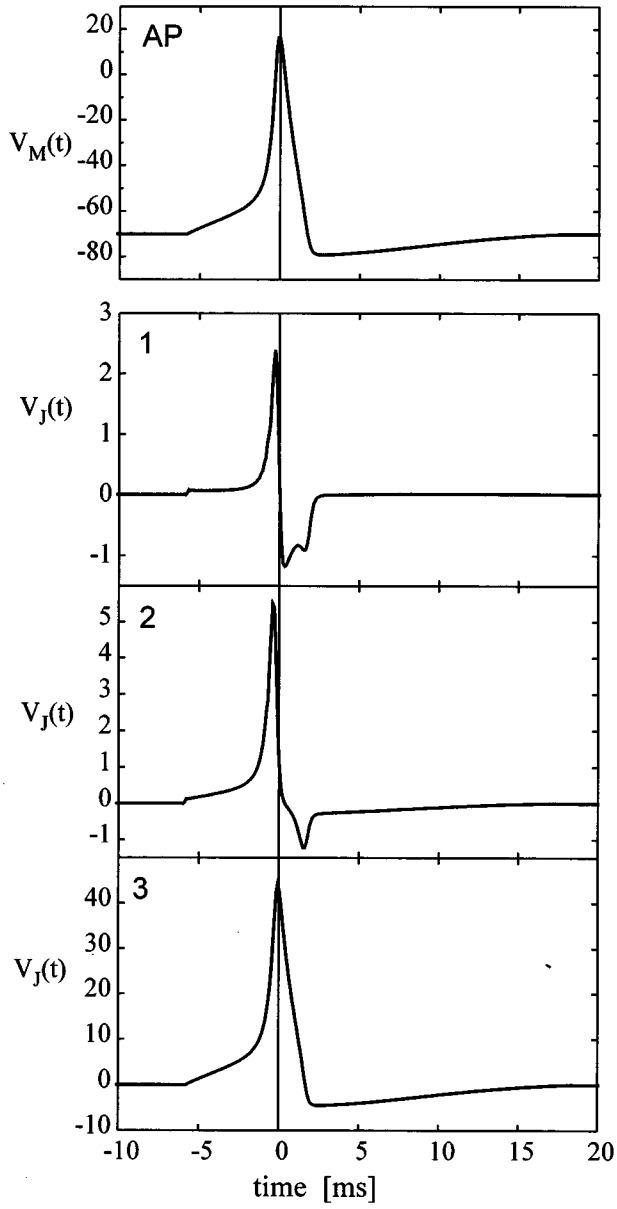

FIG. 10. Computed response to neuronal excitation. An action potential (AP) $V_M(t)$ of a Retzius cell is shown in the uppermost figure. The ac component of the voltage $V_J(t)$ in the junction is computed from the transfer function of the junctions 1, 2, and 3 parametrized by the point-contact model (Table II).

with excited neurons [2,4] and dubbed *A*-type junction. Even details of the asymmetric biphasic response of Fig. 10 correspond to the experimental results.

An almost perfect image of the action potential is computed for junction 3—without the dc background, of course. The amplitude is reduced only to about 50%. This strong and perfect coupling is due to the fact that the transfer function (Fig. 8) has a large constant amplitude and a vanishing phase over the spectral range which covers the typical frequencies of the action potential. Such a strong coupling of an action potential was observed with excited neurons on transistors [2,4] and dubbed *B*-type junction. All details of the monophasic response of Fig. 10 correspond to the experimental results. Thus the *B*-type coupling of action potentials is not due an extremely high value of the seal resistance as

proposed [2]. The high amplitude of the transfer function at low frequencies is caused by a low resistance of the membrane.

The response of junction 2 is between that of junction 1 and 3. The signal is biphasic as in junction 1 but has a distinctly higher amplitude. Also that kind of response is observed sometimes with excited neurons (*AB*-type junction).

It may be surprising that the effect of an action potential can be described by the transfer function of the linear regime. The result indicates that the membrane in the junction is quasistatic, i.e., that it has lost its nonlinear properties which give rise to the action potential in the free part of the membrane. The modifications of the attached membrane—as indicated by the changed conductance—are frozen on the time scale of the action potential.

V. CONCLUSIONS

We determined the transfer of ac signals from neurons to transistors within the regime of linear response up to 5000 Hz and measured simultaneously the impedance of the neurons. For an interpretation we used the concept of a ''sandwich cable'' at the interface of a nerve cell and a silicon chip. This cable is two-dimensional, driven from one side and grounded at its periphery. We considered two models, a homogeneous circular plate contact and an equivalent point contact.

We found that neuron-silicon junctions differ in the resistance of the attached membrane and of the seal resistance between membrane and oxidized silicon. Two kinds of junctions predominate, those with a leaky seal and an unmodified membrane and those with an enhanced seal and a membrane with rather low resistance. These two types are represented by the junctions 1 and 3, respectively, in the present study. The transfer functions of the junctions allow us to compute the ac coupling of an action potential of excited neurons. They are in perfect correspondence to a weak biphasic response (*A* type) and the strong monophasic response (*B* type) as reported in previous papers [2,4].

The conceptual basis for the discrete nature of neuron-silicon junctions is not known. We cannot predict the type of junction formed from the procedure of assembly. It may be mentioned, however, that we observe sometimes transitions from an *A* type to a *B* type by pressing the neuron onto the chip by an impaled electrode. It is possible even to induce reversible transitions between an *A* type and a *B* type by periodically changing the applied pressure [15].

A more detailed analysis of the adhesion region may lead to a full rationalization of neuron transistors. One approach will be the use of many transistors in the same junction such that the electrical features of the two-dimensional cable are revealed. A first step into that direction was reported in a recent note [5]. Of crucial importance will be a study of the structure of the junctions, in particular of the distance between membrane and silicon dioxide. The method of fluorescence interferometry as suggested recently may solve that problem [6]. Further tools will be the control of ion channels in the junction by a variation of the holding voltage, by an application of specific drugs and by genetic transfection of the cells.

ACKNOWLEDGMENTS

We thank Adolf Kuttruff for his support with electronic problems. The project was supported by the Deutsche Forschungsgemeinschaft (Grant Fr 349/9).

[1] P. Fromherz, Ber. Bunsenber. Phys. Chem. **100**, 1093 (1996).
[2] P. Fromherz, A. Offenhäusser, T. Vetter, and J. Weis, Science **252**, 1290 (1991).
[3] P. Fromherz and A. Stett, Phys. Rev. Lett. **75**, 1670 (1995).
[4] P. Fromherz, C. O. Müller, and R. Weis, Phys. Rev. Lett. **71**, 4079 (1993).
[5] R. Weis, B. Müller, and P. Fromherz, Phys. Rev. Lett. **76**, 327 (1996).
[6] A. Lambacher and P. Fromherz, Appl. Phys. A **63**, 207 (1996).
[7] P. Bergveld, J. Wiersma, and H. Meertens, IEEE Trans. Biomed. Eng. **23**, 136 (1976).
[8] D. T. Jobling, J. G. Smith, and H. V. Wheal, Med. Biol. Eng. Comput. **19**, 553 (1981).
[9] A. L. Hodgkin and A. F. Huxley, J. Physiol. (London) **117**, 500 (1952).
[10] J. J. B. Jack, D. Noble, and R. W. Tsien, *Electric Current Flow in Excitable Cells* (Clarendon, Oxford, 1985).
[11] P. Fromherz, Biochim. Biophys. Acta **986**, 341 (1989).
[12] P. Fromherz, Phys. Rev. E **52**, 1203 (1995).
[13] I. D. Dietzel, P. Drapeau, and J. G. Nicholls, J. Physiol. (London) **372**, 191 (1986).
[14] O. P. Hamill, A. Marty, E. Neher, B. Sakmann, and F. J. Sigworth, Pflügers Arch. **391**, 85 (1981).
[15] M. Jenkner and P. Fromherz (unpublished).